

# Synergistic catalytic hydrogenation of phenol over hybrid nano-structure Pd catalyst

Yanji Zhang, Jicheng Zhou\*, Kai Li, Mengdie Lv

Key Laboratory of Green Catalysis and Chemical Reaction Engineering of Hunan Province, School of Chemical Engineering Xiangtan University, Xiangtan 411105, Hunan Province, China

## ARTICLE INFO

### Keywords:

Synergistic catalysis  
Hybrid nano-structure catalyst  
Zirconia  
Selective hydrogenation  
Photochemical route

## ABSTRACT

Pd-based catalyst is one of the most widely used catalysts in the selective hydrogenation of phenol. Herein, a new strategy has been developed to fabricate a hybrid nano-structure Pd catalyst. By coating  $ZrO_2$  on the activated carbon(AC), then anchored Pd nanoparticles on the  $ZrO_2/AC$ , a hybrid nano-structure Pd/@- $ZrO_2/AC$  catalyst with strong synergy can be obtained. The results show that the Pd/@- $ZrO_2/AC$  catalyst exhibited a synergistic effect and remarkable catalytic activity in the selective hydrogenation of phenol, outperforming both conventional Pd/ $ZrO_2$  and Pd/AC catalyst. Importantly, the catalytic activity was closely related to the calcination temperature of  $ZrO_2/AC$ . The  $ZrO_2/AC$  support was calcined at 500°C with a minimum particle size, which enables Pd nanoparticles to support on it with high dispersion. Then the Pd/@- $ZrO_2/AC(500)$  exhibited stronger interaction of Pd nanoparticles with the  $ZrO_2/AC$  surface as compared to other catalysts and shown the highest catalytic activity. Moreover, a series of this hybrid nano-structure Pd/@- $Me_xO_y/AC$  catalysts( $Me_xO_y$ :  $TiO_2$ ,  $CeO_2$ ,  $La_2O_3$ ) have been synthesized and further confirmed the synergistic effect in the selective hydrogenation.

## 1. Introduction

Catalyzed hydrogenation reactions have attracted the attention of researchers because of their importance in the industrial production of chemicals and fuels [1]. Supported metal catalysts are notable for their high catalytic performance [2,3], while the hydrogenation of other unsaturated functional groups was unavoidable [4].

Taking phenol hydrogenation as an example, cyclohexanone is an important precursor to prepare caprolactam and adipic acid, which are the main ingredients for the synthesis of Nylon 6 and Nylon 66 [5]. Much attention has been given to developing an efficient catalyst for one-step selective hydrogenation of phenol to cyclohexanone [6,7]. In the past decades, researchers have reported a variety of strategies to design highly active catalysts, mainly in: (i) adding auxiliaries or modifiers. The most common method is to add an alkali metal to increase the selectivity of the catalyst [[8–10]]. Han and Jiang et al. reported a dual-supported Pd@C Lewis acid catalyst in the hydrogenation of phenol and attained a complete phenol conversion with > 99.9% selectivity to cyclohexanone under mild conditions. Pillai et al. [10]

found that Sr-promotion enhanced the basicity of the Pd catalyst, thereby increasing the selectivity of cyclohexanone. (ii) Improve atomic utilization. The particle size and dispersibility of metal play a vital role in catalytic performance [11–13]. Li et al. [13] reported a Pd@FDU-N catalyst, which showed excellent catalytic activity and cyclohexanone selectivity. They pointed out that the reason for the better performance of the catalyst is the N modified mesopores carbon material can greatly improve the dispersion of Pd particles. (iii) The structure of the catalyst. One type was based on the support, the carbon-supported catalyst was the most widely used catalysts [14,15]. Rode et al. [15] prepared a series of catalysts(Rh/C, Ru/C, Pd/C, and Pt/C). The study found that the phenol conversion was 35% and 11% by Rh/C and Ru/C catalyst, respectively. And the phenol conversions were less than 1% by Pd/C and Pt/C catalyst, but the cyclohexanone selectivity was about 20% promotion. They concluded that when the Rh or Ru as catalyst activity group, it was easy to produce the whole hydrogenation product cyclohexanol, but when the Pd or Pt as catalyst activity group, higher selectivity of cyclohexanone will be achieved. With the continuous development, more new materials are emerging, such as carbon nano-

\* Corresponding author.

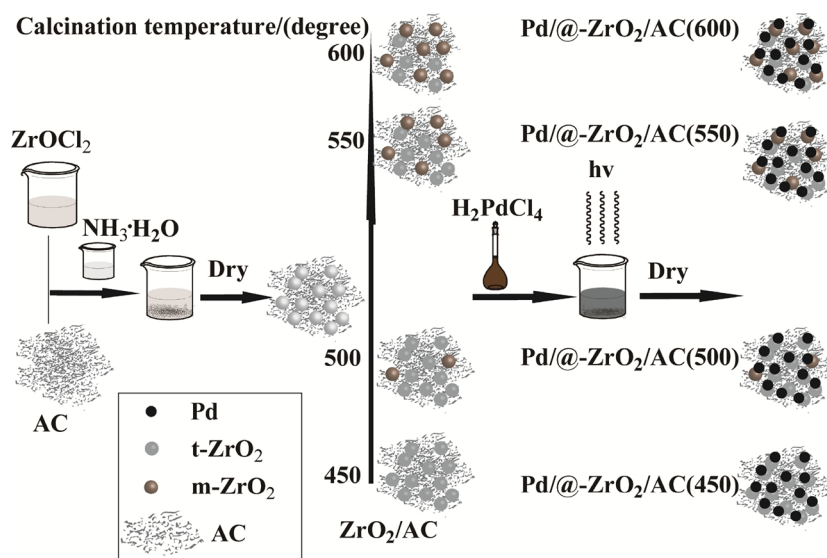
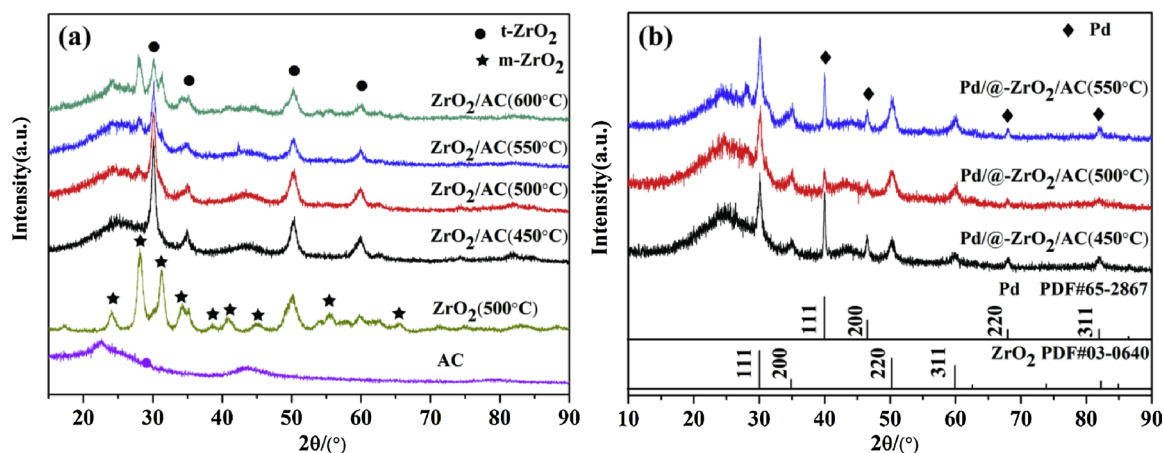
E-mail addresses: [zhoujicheng2012@126.com](mailto:zhoujicheng2012@126.com), [zhoujicheng@sohu.com](mailto:zhoujicheng@sohu.com) (J. Zhou).

<https://doi.org/10.1016/j.mcat.2019.110567>

Received 27 June 2019; Received in revised form 16 August 2019; Accepted 16 August 2019

Available online 23 August 2019

2468-8231/ © 2019 Elsevier B.V. All rights reserved.

Scheme 1. The synthetic procedure of Pd/@-ZrO<sub>2</sub>/AC.Fig. 1. XRD patterns of ZrO<sub>2</sub>/AC with different calcination temperatures (a) and Pd/@-ZrO<sub>2</sub>/AC(450-550) samples (b).

tube(CNT), nitrogen-doped carbon(CN), zeolite and metal-organic frameworks. In addition [16–19], metal oxides have been studied as supports for many years, especially those containing acid-base property were widely used, the most commonly used was TiO<sub>2</sub> [20,21], CeO<sub>2</sub> [22,23], SiO<sub>2</sub> [24–26], and Al<sub>2</sub>O<sub>3</sub> [26,27]. But the performance of such a conventional metal-supported catalyst directly on the oxide was far from satisfactory. Because of the high surface area, fascinating electronic, and textural properties of the specially structured metal oxide [28], thus researchers have gradually made the oxide into a special morphology such as mesoporous or tubular nanorods to improve the catalytic performance [29,30]. From these metal/support catalyst, the researchers found the synergistic effect/metal-support interaction, which enhanced metal dispersion [22], adjusted the electronic state of catalyst surface [23,28,30], and improve reaction rate, then increase catalytic activity and selectivity for target product. The other type is to fabricate a catalyst composed of the multi-component composite. The

researchers [31] found that adding Ru could effectively improve the Pd dispersion and promote the electronic interaction between the Pd and Ru, both of which contribute to enhancing the catalytic activity. Summary, most of the reported catalysts was supported the metal on the single support directly, then by improving the support or adding other elements to improve the activity of the catalyst.

In this work, we proposed a new strategy to fabricate a hybrid nanostructure Pd/@-ZrO<sub>2</sub>/AC catalyst, which utilized the principle of spontaneous single layer dispersion to coat nano-ZrO<sub>2</sub> on the activated carbon(AC), then loaded Pd nanoparticles on the ZrO<sub>2</sub>/AC by a photochemical route at room temperature. To our knowledge, only one group [32] used ZrO<sub>2</sub> as a support for the hydrogenation of phenol, they prepared a Pd/ZrO<sub>2</sub>-MS catalyst with mesoporous ZrO<sub>2</sub> to improve the activity, then obtained lower phenol conversion (62.9%) but very high selectivity of cyclohexanone (93%). The activity of this Pd/ZrO<sub>2</sub>-MS catalyst was unsatisfactory. Unlike the traditional catalysts (Pd

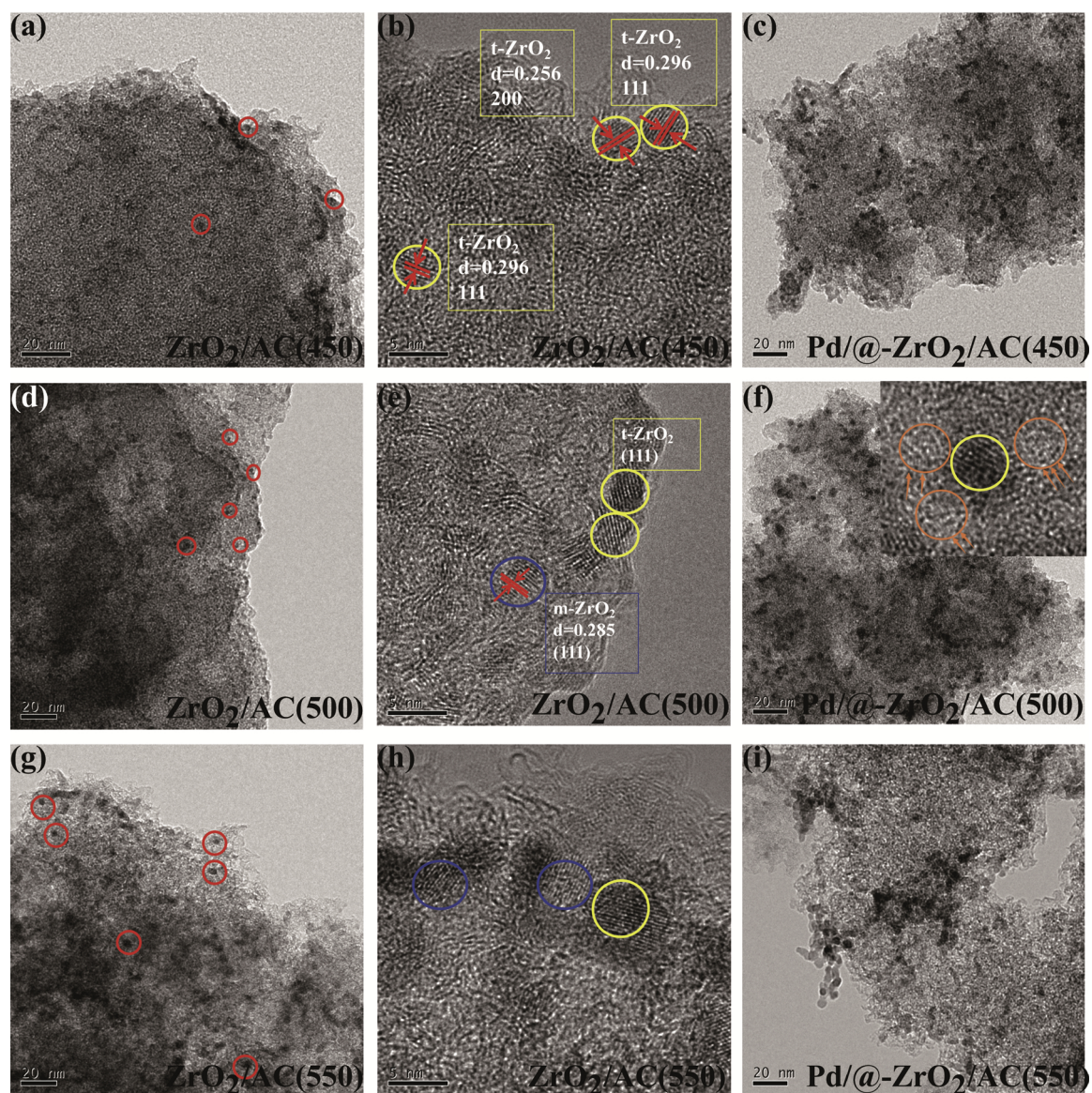


**Fig. 2.** TEM and HR-TEM images of ZrO<sub>2</sub>/AC(450) (a–b) and Pd/@-ZrO<sub>2</sub>/AC(500)(c); ZrO<sub>2</sub>/AC(500) (d–e) and Pd/@-ZrO<sub>2</sub>/AC(500)(f); ZrO<sub>2</sub>/AC(550) (g–h) and Pd/@-ZrO<sub>2</sub>/AC(550)(i). Yellow, blue and orange circle represent t-ZrO<sub>2</sub>, m-ZrO<sub>2</sub> and Pd, respectively. (For interpretation of the references to colour in this figure legend, the reader is referred to the web version of this article).

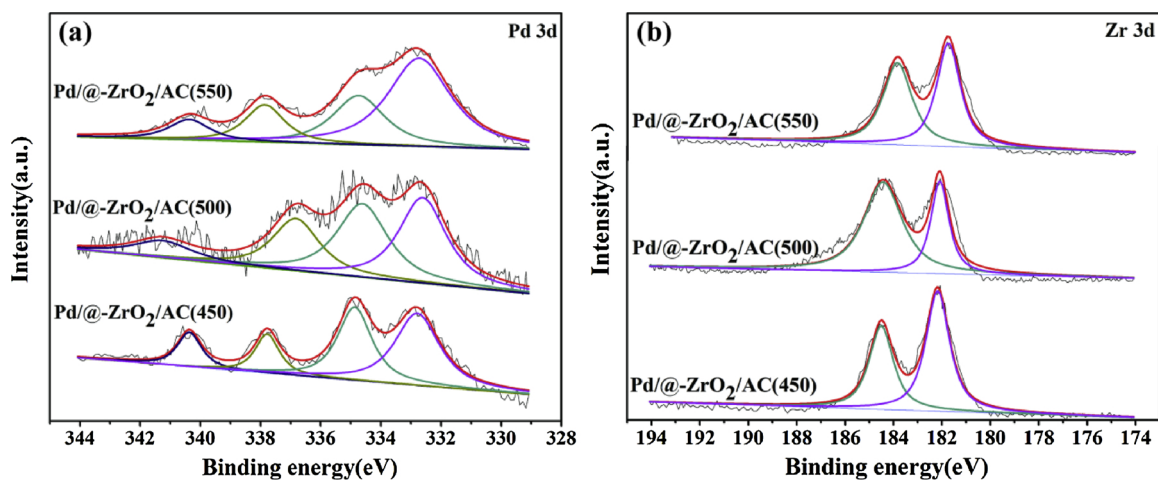


**Fig. 3.** XPS profiles of Pd/@-ZrO<sub>2</sub>/AC (a) Pd 3d spectra and (b) Zr 3d spectra.

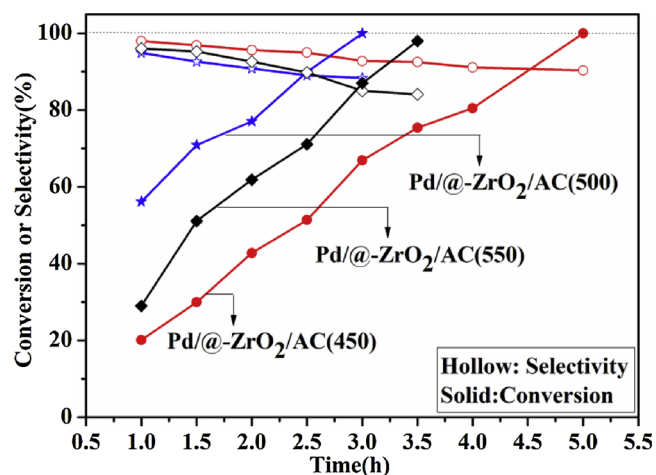


Fig. 4. Hydrogenation of phenol on Pd/@-ZrO<sub>2</sub>/AC(450), Pd/@-ZrO<sub>2</sub>/AC(500) and Pd/@-ZrO<sub>2</sub>/AC(550). Reaction conditions: 0.1 g cat., 0.353 g phenol, 20 mL H<sub>2</sub>O, 80°C, 0.7 MPa.

loaded on single support directly), our hybrid nano-structure catalyst had a nano-ZrO<sub>2</sub> layer which played an important role in this catalyst and shown a synergistic effect between Pd and ZrO<sub>2</sub>/AC. The Pd/@-ZrO<sub>2</sub>/AC catalyst demonstrated outstanding activity than that of traditional Pd/ZrO<sub>2</sub> and Pd/AC catalyst.

## 2. Experimental

### 2.1. Catalyst preparation

Pretreatment of AC with acid. A commercial activated carbon made from coconut shells (Fujian Xinsen Carbon Co. Ltd.) was pretreated with HNO<sub>3</sub> (10%) under refluxing at 60°C for 2 h. Then the AC was cooled to room temperature, washed to neutrality with deionized water. Finally, the AC was dried at 120°C.

Preparation of ZrO<sub>2</sub>/AC. 1.453 g of ZrOCl<sub>2</sub>·8H<sub>2</sub>O was dissolved in 50 mL deionized water, then added the pre-processed AC(5 g) in the solution under stirring, 1.5 mol/L NH<sub>3</sub>·H<sub>2</sub>O was added dropwise until the pH of the resulting solution was 10, the mixture was vigorously stirred during the addition, after aging for 24 h, the precipitate was filtered and washed by deionized water, and then dried at 100°C followed by calcination in muffle furnace without atmosphere protection at different temperature(450-600°C) for 4 h. The obtained ZrO<sub>2</sub>/AC are referred to as ZrO<sub>2</sub>/AC(450), ZrO<sub>2</sub>/AC(500), ZrO<sub>2</sub>/AC(550) and ZrO<sub>2</sub>/

AC(600), respectively. ZrO<sub>2</sub>(500) was prepared in the same manner as ZrO<sub>2</sub>/AC(500) except that no AC was added.

Synthesis of Pd/@-ZrO<sub>2</sub>/AC. It was adapted from the method of our previous work [33–36]. As-prepared ZrO<sub>2</sub>/AC(0.582 g) was added in deionized water(100 mL) and methanol(5 mL) mix solution, add the H<sub>2</sub>PdCl<sub>4</sub>(1.5 mL, 0.012 g/mL, Chenzhou GaoXin Platinum Co., Ltd.) in it, ultrasonic dispersion for 30 min, then ultraviolet lamp(220/15 W, Guangzhou Cnlight Optoelectronics Technology Co., Ltd.) for 10 h. Finally, the sample was separated by filtration, washed by distilled water, dried in a vacuum oven at 80°C for 10 h. The synthetic procedure was illustrated in Scheme 1. The Pd content of all Pd catalysts is about 2.8 wt.% by ICP.

### 2.2. Catalyst characterization

X-ray diffraction (XRD) of samples was obtained on a Rigaku D/max-II/2500 X-ray powder diffractometer, Cu Kα radiation was employed and the working voltage and current were 40 kV and 30 mA, respectively. 2θ scans were performed from 10° to 90° at a 10°/min speed. Transmission electron microscope (TEM) images were obtained with a JEOL JEM-2100 F at an acceleration voltage of 200 kV. The samples were prepared by dispersing the catalyst powder in ethanol under ultrasonic for 15 min and then the solution was dropped on a carbon film of copper grid. X-ray photoelectron spectroscopy (XPS) was performing using ESCALAB 250Xi (Thermo) with Al Kα radiation. All the spectra measured were corrected by setting the reference binding energy of carbon (1 s) at 284.8 eV. Spectra curve fitting and quantification were performed with the XPSPEAK software. The surface composition of the samples was determined from the peak areas of the corresponding lines. The specific surface areas of the samples were calculated by the BET method by N<sub>2</sub> adsorption-desorption with a NOVA-2200e volumetric dsorption analyzer. Prior to measurement, samples were degassed under vacuum at 383 K overnight. The content of Pd in the catalysts was measured on an ICP-AES 7300DV instrument. Pd dispersions were measured by pulse adsorption of CO on a AutoChem II 2920 automated characterization system at 50°C. The samples were pretreated in a 5 vol.% H<sub>2</sub>/95 vol.% Ar flow at 673 K for 2 h. The degree of dispersion and the mean particle size were estimated from the measured CO uptake.

### 2.3. Catalyst tests

The typical procedure for hydrogenation of phenol was as follows: 0.1 g catalyst, 0.353 g phenol, and 20 mL H<sub>2</sub>O were placed in an autoclave. The autoclave(50 mL, self-made) was purged with H<sub>2</sub> to remove the air 3 times. Then the reaction was stirred at 1000 rpm under

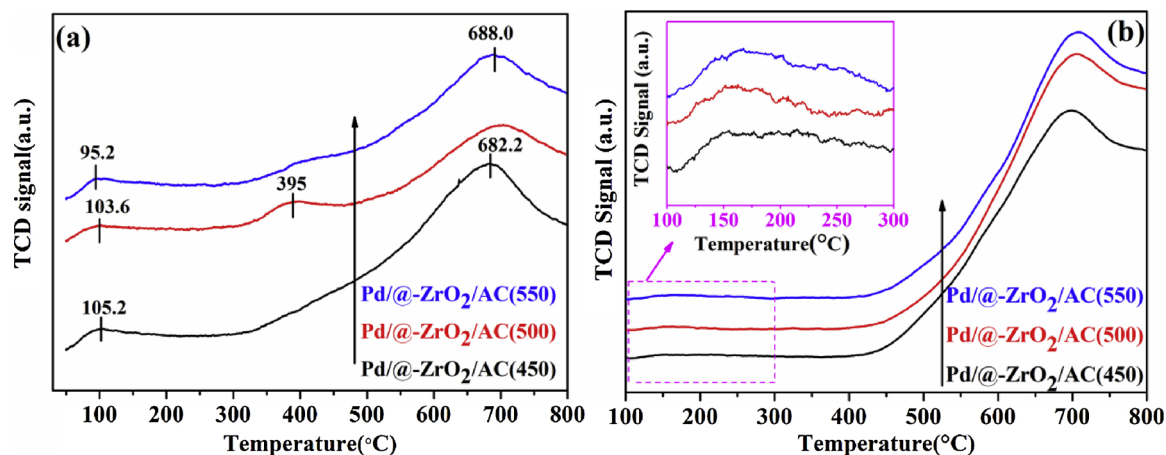


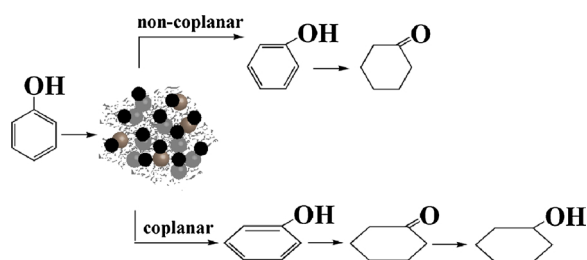
Fig. 5. The acidity and basicity properties of the Pd/@-ZrO<sub>2</sub>/AC catalyst by NH<sub>3</sub>-TPD(a) and CO<sub>2</sub>-TPD(b).

**Table 1**  
The acidic properties of the Pd/@-ZrO<sub>2</sub>/AC catalyst by NH<sub>3</sub>-TPD.

Catalyst	70–250°C		250–500°C		> 500°C		Total n <sub>NH3</sub> (μmol/g)
	Peak temperature (°C)	n <sub>NH3</sub> (μmol/g)	Peak temperature(°C)	n <sub>NH3</sub> (μmol/g)	Peak temperature(°C)	Desorbed NH <sub>3</sub> (μmol/g)	
Pd/@-ZrO <sub>2</sub> /AC(450)	105.2	284.1	–	–	682.2	4137.0	4421.1
Pd/@-ZrO <sub>2</sub> /AC(500)	103.6	183.7	395.0	481.7	707.1	2193.9	2859.3
Pd/@-ZrO <sub>2</sub> /AC(550)	95.2	259.7	–	–	688.0	3167.1	3126.8

**Table 2**  
The basicity properties of the Pd/@-ZrO<sub>2</sub>/AC catalyst by CO<sub>2</sub>-TPD.

Catalyst	100–200°C		600–800°C		Total n <sub>CO2</sub> (μmol/g)
	Peak temperature(°C)	n <sub>CO2</sub> (μmol/g)	Peak temperature(°C)	n <sub>CO2</sub> (μmol/g)	
Pd/@-ZrO <sub>2</sub> /AC(450)	153.2	17.0	700.19	1705.3	1722.3
Pd/@-ZrO <sub>2</sub> /AC(500)	156.0	7.6	704.59	1790.9	1798.5
Pd/@-ZrO <sub>2</sub> /AC(550)	167.8	17.1	709.68	1708.8	1725.9



**Scheme 2.** Possible reaction mechanism of phenol over Pd/@-ZrO<sub>2</sub>/AC(500).

H<sub>2</sub> pressure until the temperature reached 70°C. After the end of the reaction, the autoclave was cooled to room temperature, then the products were analyzed using an Agilent 6890 N GC with an HP-5 capillary column and FID detector.

### 3. Results and discussion

#### 3.1. Characterization

XRD patterns of AC, ZrO<sub>2</sub>, ZrO<sub>2</sub>/AC support and Pd/@-ZrO<sub>2</sub>/AC catalyst are compared in Fig. 1. All samples present broadened peaks at 22.6° and 43.3°, which could be attributed to the AC. From Fig. 1(a), the peaks at 2θ of 30.2°, 35.0°, 50.4° and 60.0° for the samples are readily

assigned to tetragonal ZrO<sub>2</sub> (t-ZrO<sub>2</sub>)(JCPD 03-0640), the peaks at 2θ of 24.1°, 27.9°, 31.4°, 34.1°, 38.4°, 40.4°, 45.1°, 55.3°, and 65.2° are assigned to monoclinic ZrO<sub>2</sub> (m-ZrO<sub>2</sub>)(JCPD 01-0750). The pure ZrO<sub>2</sub>(500) exhibited a large amount of m-ZrO<sub>2</sub>, but the ZrO<sub>2</sub>/AC calcined at 500°C was mainly composed of t-ZrO<sub>2</sub>. This phenomenon indicated that AC could affect the phase transformation temperature of ZrO<sub>2</sub>. It can be seen that calcination of ZrO<sub>2</sub>/AC at 500°C and 600°C led to the partial transformation of t-ZrO<sub>2</sub> into m-ZrO<sub>2</sub>. BET measurements revealed that the specific surface areas of ZrO<sub>2</sub>/AC(450), ZrO<sub>2</sub>/AC(500), ZrO<sub>2</sub>/AC(550) and ZrO<sub>2</sub>/AC(600) were 1078.7m<sup>2</sup>/g, 1183.4m<sup>2</sup>/g, 1297.1m<sup>2</sup>/g, and 910.5m<sup>2</sup>/g, respectively. Although the specific surface area of t-ZrO<sub>2</sub> was usually higher than that of m-ZrO<sub>2</sub> [37], the ZrO<sub>2</sub> was located on AC (the ZrO<sub>2</sub> content was about 10 wt.%) and the calcining process has the effect of expanding the pores of AC, the higher temperature, the more obvious reaming effect. So, as the calcination temperature increased, the specific surface area of ZrO<sub>2</sub>/AC(450–550) also increased, except ZrO<sub>2</sub>/AC(600). Because the AC was not resistant to high temperature under the non-atmosphere protection condition. When the ZrO<sub>2</sub>/AC(600) was taken out of the muffle furnace, it can be clearly seen that the surface has a layer of gray-white substances, apparently, part of the AC was burned into ash. From the XRD patterns of ZrO<sub>2</sub>/AC(600), it could also be seen that the diffraction peak of AC at about 2θ = 43° was weakened because high temperature destroyed the AC). The XRD pattern of Pd/@-ZrO<sub>2</sub>/AC was shown in Fig. 1(b), some weak peaks that appeared at 2θ = 40.1°, 46.6°, 68.1°,

**Table 3**  
Hydrogenation of phenol over Pd-based catalysts.

Catalyst	Reaction condition (m(cat.)/m(phenol)/min/°C/MPa)	TOF <sup>a</sup> (h <sup>-1</sup> )	Con. (%)	Sel. (%)		Note
				C=O	–COH	
ZrO <sub>2</sub> /AC(500)	0.1 g/0.353 g/180/80/0.7	–	–	–	–	This work
2.8%Pd/AC	0.1 g/0.353 g/180/80/0.7	–	31.8	88.7	11.3	This work
2.8%Pd/ZrO <sub>2</sub> (500)	0.1 g/0.353 g/180/80/0.7	–	7.4	97.7	2.3	This work
2.8%Pd/@-10%ZrO <sub>2</sub> /AC(450)	0.1 g/0.353 g/300/80/0.7	92.8	100	90.3	9.7	This work
2.8%Pd/@-10%ZrO <sub>2</sub> /AC(500)	0.1 g/0.353 g/180/80/0.7	222.3	100	88.3	11.7	This work
2.8%Pd/@-10%ZrO <sub>2</sub> /AC(550)	0.1 g/0.353 g/210/80/0.7	133.3	98.0	84.1	15.9	This work
2.8%Pd/@-5%ZrO <sub>2</sub> /AC(500)	0.1 g/0.353 g/180/80/0.7	–	71.6	91.0	9.0	This work
2.8%Pd/@-8%ZrO <sub>2</sub> /AC(500)	0.1 g/0.353 g/180/80/0.7	–	88.6	91.4	8.6	This work
2%Pd/MOF140-AA	0.2 g/1 g/120/260/2	–	98.3	14.3	40.1	[19]
2%Pd-UiO-66	0.0066 g/0.0066 g/120/120/0.2	–	100	< 5	90	[42]
2.92%Pd/N <sub>4,8</sub> -meso-CNRs	0.053 g/0.047 g/180/40/0.1	–	93.2	97.3	2.7	[43]
5%Pd@FDU – N	-/0.5 mmol/60/100/0.1	–	80	> 99	< 1	[15]
0.9%Pd/Amberlyst-45	-/0.5 mmol/30/60/1	118	82.5	65.7	34.3	[44]

<sup>a</sup> TOF = Moles of reactant/(load of Pd × m(cat.) × Pd dispersion × reaction time/106.42). The Pd dispersion of Pd/@-ZrO<sub>2</sub>/AC(450), Pd/@-ZrO<sub>2</sub>/AC(500), and Pd/@-ZrO<sub>2</sub>/AC(550) were 38%, 36%, and 31%, respectively. Calculated by CO pulse chemisorption.

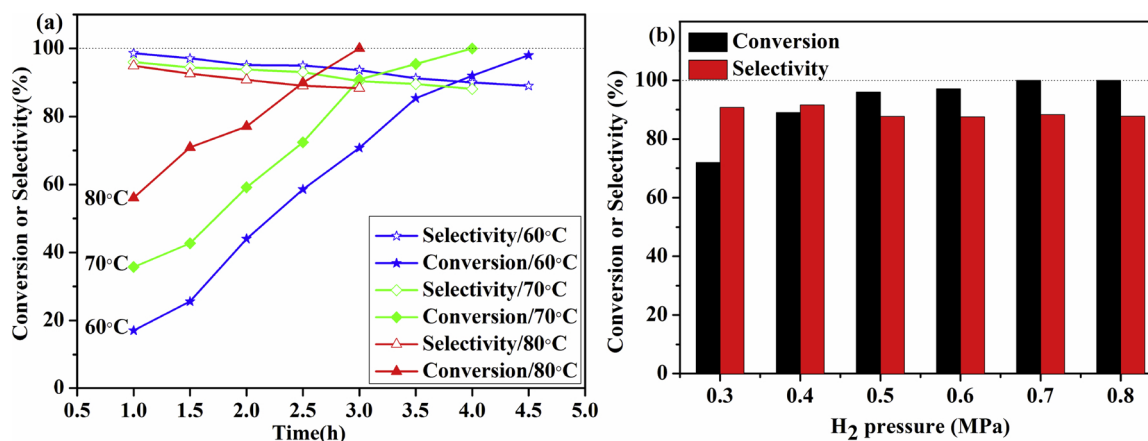


Fig. 6. Hydrogenation of phenol on Pd/@-ZrO<sub>2</sub>/AC(500) with different reaction temperatures(a); and different H<sub>2</sub> pressure(b).

and 82.5° were attributed to the Pd(JCPD 65-2867).

The results of the TEM and HR-TEM analysis were shown in Fig. 2. The ZrO<sub>2</sub> on the AC with different calcination temperature had a different size. For ZrO<sub>2</sub>/AC(450) (Fig. 2a–b), it has shown interplanar spacings of 0.256 nm and 0.296 nm corresponding to the (200), and (111) planes of t-ZrO<sub>2</sub>, respectively. For ZrO<sub>2</sub>/AC(500) and ZrO<sub>2</sub>/AC(550) (Fig. 2d–e), it illustrated that the m-ZrO<sub>2</sub> and t-ZrO<sub>2</sub> occurred simultaneously, which was supportive of the XRD observations. Moreover, it could be clearly observed from Fig. 2(a, d, g, red circle) that the average particle size of ZrO<sub>2</sub> in ZrO<sub>2</sub>/AC(500) was smaller than that of ZrO<sub>2</sub>/AC(450) and ZrO<sub>2</sub>/AC(550). For Pd/@-ZrO<sub>2</sub>/AC(500) (Fig. 2f), the lattice fringes with an interplanar spacing of 0.194 nm were visible (Fig. 2f, inside, orange circle), which was ascribed to the (200) crystal plane of Pd. As can be seen, it was difficult to distinguish the Pd nanoparticles and ZrO<sub>2</sub> from Fig. 2c, f, i, so the size analysis of Pd nanoparticles could not be achieved from TEM.

The XPS analysis of Pd/@-ZrO<sub>2</sub>/AC was shown in Fig. 3. Peaks detected at around 334.7 ± 0.1 eV and 340.8 ± 0.4 eV can be readily assigned to the Pd 3d<sub>5/2</sub> and Pd 3d<sub>3/2</sub> electronic states of Pd(0) [38], compared with standard values(335 eV and 340.3 eV), there was a difference between the measured value and the standard value, means the strong metal-support interaction between nano-Pd and ZrO<sub>2</sub>/AC. Particularly, the peaks of Pd for Pd/@-ZrO<sub>2</sub>/AC(500) has the largest difference from the standard value, indicating that the highest interaction between Pd and ZrO<sub>2</sub>/AC(500). The binding energies of Pd 3d<sub>5/2</sub> were found to be 337.8 eV, 336.8 eV and 337.9 eV for Pd/@-ZrO<sub>2</sub>/AC(450), Pd/@-ZrO<sub>2</sub>/AC(500) and Pd/@-ZrO<sub>2</sub>/AC(550), respectively, which corresponded to the Pd<sup>2+</sup> species. The presence of Pd<sup>2+</sup> species was probably due to the interaction of Pd and surface adsorbed oxygen [39]. As we can see, Pd 3d<sub>5/2</sub> was partially overlapped with Zr 3p<sub>3/2</sub> in the XPS spectra in Fig. 3(a), the Zr 3d XPS spectra were shown in Fig. 3(b), two signals were observed at values of binding energy around 182.2 eV and 184.5 eV, which could be assigned to the formation of traces of Zr 3d<sub>5/2</sub> and Zr 3d<sub>3/2</sub>, respectively [40].

### 3.2. Hydrogenation of phenol

Considering that the change of the calcination temperature of ZrO<sub>2</sub>/AC leads to the phase transition from t-ZrO<sub>2</sub> to m-ZrO<sub>2</sub>, we first used

ZrO<sub>2</sub>/AC(450), ZrO<sub>2</sub>/AC(500) and ZrO<sub>2</sub>/AC(550) as support to investigate the effect on the reaction conversion, as illustrated in Fig. 4. It can be seen that the Pd/@-ZrO<sub>2</sub>/AC(450), Pd/@-ZrO<sub>2</sub>/AC(500) and Pd/@-ZrO<sub>2</sub>/AC(550) catalyst exhibited 66.9%, 100% and 87% phenol conversion within 3 h, respectively. The Pd/@-ZrO<sub>2</sub>/AC(450) and Pd/@-ZrO<sub>2</sub>/AC(550) catalyst can be total conversion until prolong the time to 5 h and 3.5 h, respectively. These results showed that the activity of Pd/@-ZrO<sub>2</sub>/AC(500) catalyst was higher than that of Pd/@-ZrO<sub>2</sub>/AC(450) and Pd/@-ZrO<sub>2</sub>/AC(550) catalysts. For comparison, the Pd/@-ZrO<sub>2</sub>/AC(600) was also used as a reference catalyst under the same reaction condition, it only obtained 45.2% phenol conversion. Because partial AC was destroyed in 600°C, so that ZrO<sub>2</sub> was not evenly laid on the AC in ZrO<sub>2</sub>/AC(600), Pd/@-ZrO<sub>2</sub>/AC(600) may consist of Pd/ZrO<sub>2</sub> and part of Pd/@-ZrO<sub>2</sub>/AC. Therefore, Pd/@-ZrO<sub>2</sub>/AC(600) shows the lowest activity. This result demonstrated that only hybrid nano-structure Pd catalysts can exhibit synergistic catalysis and remarkable catalytic performances for the hydrogenation of phenol.

For the Pd/@-ZrO<sub>2</sub>/AC(450-550), the conversion followed the order: Pd/@-ZrO<sub>2</sub>/AC(500) > Pd/@-ZrO<sub>2</sub>/AC(550) > Pd/@-ZrO<sub>2</sub>/AC(450). According to the XPS, the Pd/@-ZrO<sub>2</sub>/AC(500) exhibited the highest interaction between Pd and ZrO<sub>2</sub>/AC(500).

In addition, the different calcination temperatures of ZrO<sub>2</sub>/AC lead to different acidity and basicity in the Pd/@-ZrO<sub>2</sub>/AC(450-550) catalysts. The NH<sub>3</sub>-TPD and CO<sub>2</sub>-TPD measurements were carried out (Fig. 5, Tables 1, 2). From Tables 1, 2, the total amount of acidity sites is in the order of Pd/@-ZrO<sub>2</sub>/AC(450) > Pd/@-ZrO<sub>2</sub>/AC(550) > Pd/@-ZrO<sub>2</sub>/AC(500). And the total basicity sites is in the order of Pd/@-ZrO<sub>2</sub>/AC(500) > Pd/@-ZrO<sub>2</sub>/AC(550) > Pd/@-ZrO<sub>2</sub>/AC(450). As we all know, the basic sites of catalyst were predominantly adsorbed phenol by “non-coplanar” which was more advantageous for the production of cyclohexanone, and the phenol was adsorbed by “coplanar” in acidity sites, cyclohexanone was not dissociation of the active site, so it was further hydrogenation for cyclohexanol [41]. Combined with reaction results, two possible pathways for the hydrogenation of phenol was proposed over the Pd/@-ZrO<sub>2</sub>/AC(450-550) catalysts (Scheme 2). Therefore, the product contains cyclohexanone and cyclohexanol.

Table 3 displays the catalytic properties of Pd-based catalysts for the hydrogenation of phenol under the same reaction condition. As can be seen, no reaction took place in the presence of ZrO<sub>2</sub>/AC(500), when Pd/

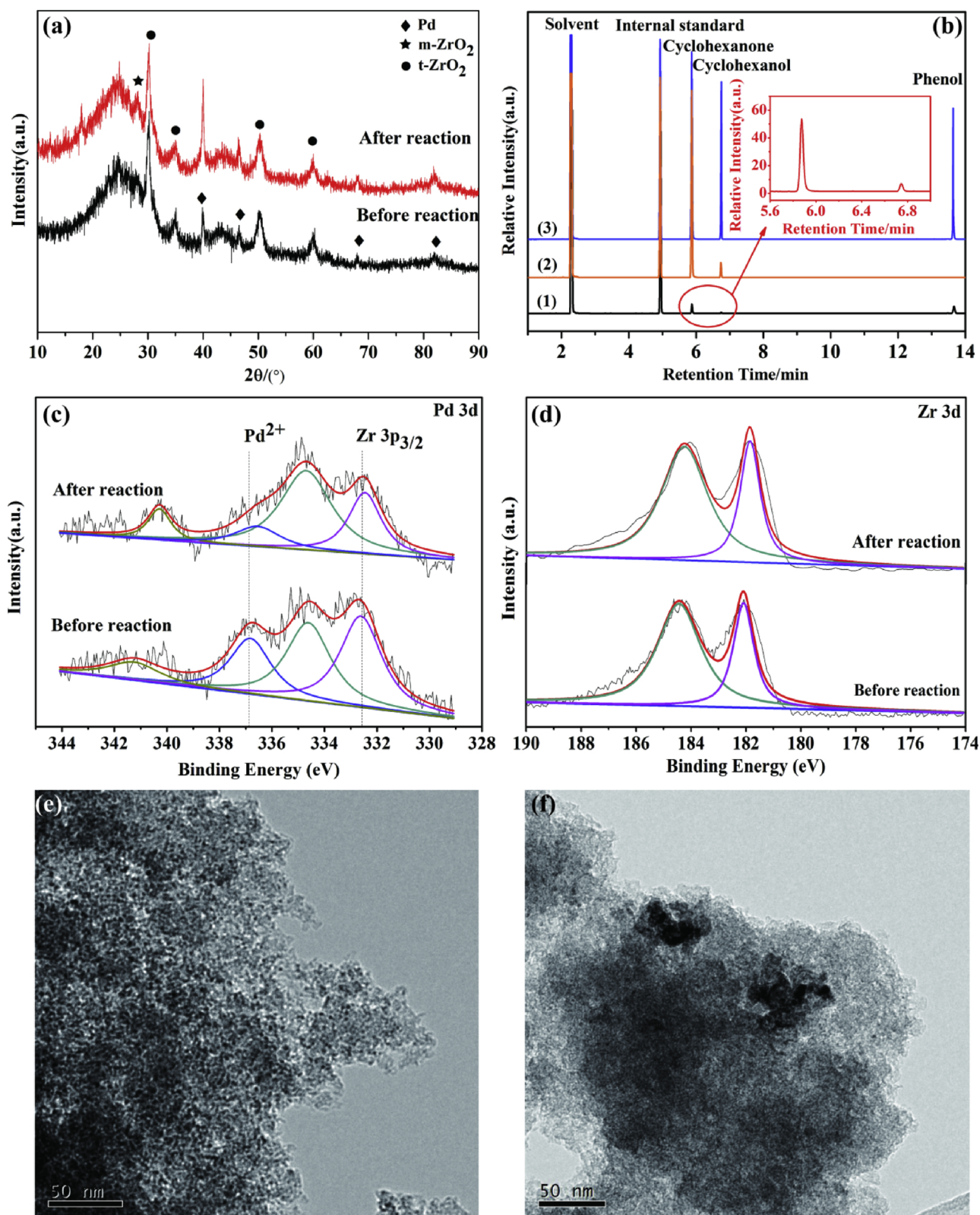


Fig. 7. The characterized of Pd/@-ZrO<sub>2</sub>/AC(500) catalyst before and after reaction (a) XRD spectra; (b) GC spectra of a solution obtained by washing the used catalyst with deionized water (1) and reaction liquid (2) (Table 2, Entry 4) and the preparation of solution (3); (c) XPS Pd 3d spectra and (d) XPS Zr 3d spectra; the TEM of Pd/@-ZrO<sub>2</sub>/AC(500) catalyst before (e) and after reaction (f).

**Table 4**  
Physical properties of Pd/@-ZrO<sub>2</sub>/AC(500) catalyst before and after reaction.

Sample	N <sub>2</sub> absorption-desorption		Pd/B.E(eV)			
	Surface area(m <sup>2</sup> /g)	V(cm <sup>3</sup> /g)	Pd <sup>+2</sup>	Pd <sup>0</sup>	Pd <sup>2+</sup> /Pd <sup>0</sup> (%)	
Fresh	1109	0.6	336.8	341.2	334.6	34.1/65.9
Used	873	0.5	336.5	340.3	334.7	16.1/83.9

AC and Pd/ZrO<sub>2</sub>(500) were applied as catalysts, the phenol conversion were 31.8% and 7.4%, respectively. Surprisingly, the catalytic activity was greatly enhanced by using Pd/@-ZrO<sub>2</sub>/AC(500) as the catalyst, phenol was completely converted. Besides, when the ZrO<sub>2</sub> loading decreased to 5 wt.% or 8 wt.%, the conversion was decreased. This result means that the ZrO<sub>2</sub> content was less than enough to cover the entire surface of the AC, the Pd nanoparticles were major anchored on the AC directly, the Pd/@-5%ZrO<sub>2</sub>/AC or Pd/@-8%ZrO<sub>2</sub>/AC consisted of major Pd/AC and slight Pd/@-ZrO<sub>2</sub>/AC. Therefore, the Pd/@-ZrO<sub>2</sub>/AC with low loading of ZrO<sub>2</sub> shown low activity. Based on the above results and characterizations, we could conclude that this hybrid nano-structure Pd/@-ZrO<sub>2</sub>/AC(500) catalyst exhibited the synergistic effect between Pd nanoparticles and ZrO<sub>2</sub>/AC support, which enhanced the activity for the hydrogenation of phenol. Compared with the recent works of the Pd catalysts, relative advantage can be obtained from our Pd/@-ZrO<sub>2</sub>/AC(500) catalyst, and the turnover frequency (TOF) based on surface Pd reached 222.3 h<sup>-1</sup>, which is higher than that of the 0.9% Pd/Amberlyst-45(118 h<sup>-1</sup>).<sup>44</sup>

Then we studied the effect of reaction conditions on phenol conversion over Pd/@-ZrO<sub>2</sub>/AC(500) catalyst. The reaction temperature (Fig. 6a) had a considerable effect on the activity of the catalyst, the phenol conversion of 100% was achieved at 0.7 MPa hydrogen pressure and 80°C for 3 h. However, even at a temperature of 60°C, 92% conversion of phenol could be reached after 4 h. It was indicated that our catalyst system could catalyze this reaction under the low reaction temperature. Moreover, when gradually increasing the pressure of hydrogen from 0.3 to 0.8 MPa, the activity was correspondingly enhanced (Fig. 6b), the selectivity slightly decreased, the increase of hydrogen pressure should enhance the solubility of hydrogen in the liquid phase and provide more active hydrogen on the surface of the catalyst, favoring the hydrogenation of the phenol.

After the reaction, the recyclability of Pd/@-ZrO<sub>2</sub>/AC(500) catalyst was investigated. The used catalyst was washed by deionized water (500 mL). Even though the phenol conversion decreased to 69.3% with the recycled catalyst, the activity of the used catalyst still higher than that of Pd/ZrO<sub>2</sub> and Pd/AC. Then the used catalyst was characterized by XRD, N<sub>2</sub> absorption-desorption, and XPS (Fig. 7 and Table 4). Compared to the diffraction peak of Pd with fresh catalyst, the diffraction peak of the used catalyst was stronger. Combined with N<sub>2</sub>

adsorption-desorption analysis (Table 4), the specific surface area of the catalyst was reduced from 1109 m<sup>2</sup>/g to 873 m<sup>2</sup>/g and pore volume is decreased from 0.6 to 0.5 cm<sup>3</sup>/g, respectively. It was indicated that the pores were clogged with organic compounds (e.g. reactants or products), or the Pd nanoparticles agglomeration. To confirm whether the organic was absorbed in the catalyst, deionized water (500 mL) was collected for washing the catalyst and extracted with ethyl acetate, then analyzed by Agilent 6890 N GC (Fig. 7b). It is shown that the major species in the solution were reactant phenol and product cyclohexanone, and slight cyclohexanol. The TEM image of the used catalyst was shown in Fig. 7f, it obvious agglomeration. Then, by calculating the integration areas of Pd<sup>0</sup> of fresh and used catalyst, it can be estimated that the percentage of Pd<sup>0</sup> was 65.9% and 83.9% (Table 4), respectively. Maybe partial Pd<sup>2+</sup> species was reduced to Pd<sup>0</sup> by hydrogen during the reaction. It demonstrates that the change of Pd valence state could not be responsible for the decrease in reaction. In addition, comparing the Zr 3d spectra of fresh and used catalyst did not reveal any changes (Fig. 7d). Therefore, the main deactivation reason of this catalyst was Pd nanoparticles agglomeration and the pores were clogged with organic compounds which may partially block the active sites, further study for the repeatability of this catalyst is still carried out.

According to this synthesis strategy of catalyst, we prepared Pd/@-CeO<sub>2</sub>/AC, Pd/@-La<sub>2</sub>O<sub>3</sub>/AC and Pd/@-TiO<sub>2</sub>/AC catalysts. These hybrid nano-structure catalysts also provide superior activity and synergistic catalysis in the hydrogenation of phenol (Fig. 8a) and benzaldehyde (Fig. 8b), outperforming the Pd/AC and Pd/metal oxide catalyst. This study opens a new direction to develop a hybrid nano-structure catalyst for heterogeneous catalytic hydrogenation reaction.

#### 4. Conclusions

In summary, a hybrid nano-structure Pd catalyst was synthesized through coating ZrO<sub>2</sub> on the AC, then loaded Pd nanoparticles on the ZrO<sub>2</sub>/AC by a photochemical route. The catalytic activity was closely related to the calcination temperature of ZrO<sub>2</sub>/AC, the ZrO<sub>2</sub>/AC support calcined at 500°C with a minimum particle size, which effects Pd nanoparticles supported on it with high dispersion, and exhibited stronger interaction of Pd nanoparticles with the ZrO<sub>2</sub>/AC surface as compared to other catalysts. The Pd/@-ZrO<sub>2</sub>/AC(500) catalyst exhibit highest activity to the hydrogenation of phenol, which was much better than that of Pd/@-ZrO<sub>2</sub>/AC(450, 550, 600) catalyst. In addition, this Pd hybrid nano-structure catalyst exhibited synergistic catalysis in selective hydrogenation, outperforming both conventional Pd/metal oxide and Pd/AC catalyst. This structure could be inferred as a feasible synthesis strategy to obtain desired metal nano-catalysts for the heterogeneous catalysis.

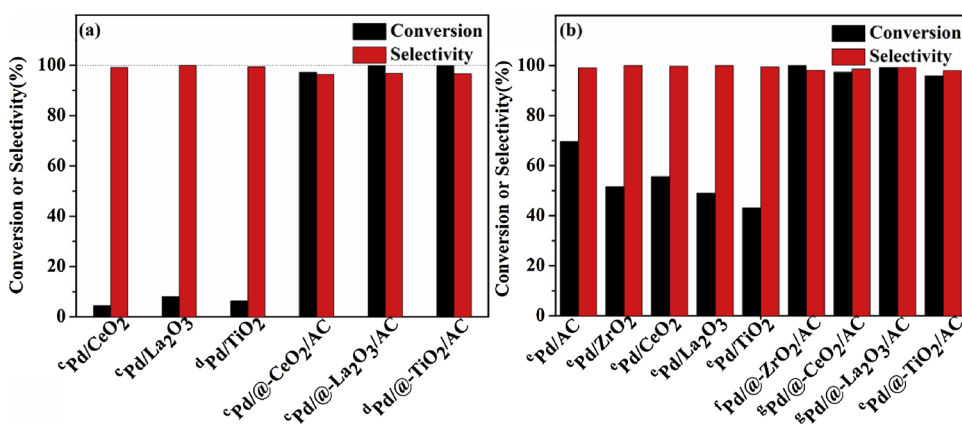


**Fig. 8.** Hydrogenation of phenol(a) and hydrogenation of benzaldehyde(b) on different catalysts. Reaction conditions: <sup>c</sup> catalyst(0.1 g), phenol(0.353 g), 70 °C, 3 h, 0.7 MPa H<sub>2</sub> pressure, H<sub>2</sub>O(20 ml); <sup>d</sup> 2 h, 0.5 MPa H<sub>2</sub> pressure; <sup>e</sup> catalyst(0.05 g), benzaldehyde(1.88 mmol), 40°C, 1 h, 0.7 MPa H<sub>2</sub> pressure, H<sub>2</sub>O(20 ml); <sup>f</sup> 30 min; <sup>g</sup> 80 min.

## Acknowledgements

This work was supported by the Natural Science Foundation of China (21676227), the Key Project of Hunan Provincial Natural Science Foundation of China (09JJ3021).

## References

- [1] J. Zhang, L. Wang, Y. Shao, Y.Q. Wang, B.C. Gates, F.S. Xiao, *Angew. Chem. Int. Ed.* 56 (2017) 9747–9751.
- [2] M. Guo, H. Li, Y.Q. Ren, X.M. Ren, Q.H. Yang, C. Li, *ACS Catal.* 8 (2018) 6476–6485.
- [3] N. Perret, X.D. Wang, L. Delannoy, C. Potvin, C. Louis, M.A. Keane, *J. Catal.* 286 (2012) 172–183.
- [4] A. Hu, X.H. Lu, D.M. Cai, H.J. Pan, R. Jing, Q.H. Xia, D. Zhou, Y.D. Xia, *Mol. Catal.* 472 (2019) 27–36.
- [5] Y. Yeohoon, R. Roger, S.W. Robert, D.H. Mei, A.L. Johannes, *J. Am. Chem. Soc.* 136 (2014) 10287–10298.
- [6] G.F. Li, J.Y. Han, H. Wang, X.L. Zhu, Q.F. Ge, *ACS Catal.* 5 (2015) 2009–2016.
- [7] C.J. Lin, S.H. Huang, N.C. Lai, C.M. Yang, *ACS Catal.* 5 (2015) 4121–4129.
- [8] H. Li, J. Liu, S.H. Xie, M.H. Qiao, W.L. Dai, Y.F. Lu, H.X. Li, *Adv. Funct. Mater.* 18 (2008) 3235–3241.
- [9] H.Z. Liu, T. Jiang, B.X. Han, S.G. Liang, Y.X. Zhou, *Science* 326 (2009) 1250–1252.
- [10] U.R. Pillai, E. Sahle-Demessie, *Appl. Catal. A-Gen.* 281 (2005) 31–38.
- [11] J.X. Zhang, G.W. Huang, C. Zhang, Q.H. He, C. Huang, X. Yang, H.Y. Song, Z.X. Liang, L. Du, S.J. Liao, *Chin. J. Catal.* 34 (2013) 1519–1526.
- [12] D.M. Zhang, Y.J. Guan, Emiel J.M. Hensen, L. Chen, Y.M. Wang, *Catal. Commun.* 41 (2013) 47–51.
- [13] Z.L. Li, J.H. Liu, C.G. Xia, F.W. Li, *ACS Catal.* 3 (2013) 2440–2448.
- [14] Y. Ma, Y.Q. Huang, Y.W. Cheng, L.J. Wang, X. Li, *Catal. Commun.* 57 (2014) 40–44.
- [15] C.V. Rode, U.D. Joshi, O. Sato, M. Shirai, *Chem. Commun* 9 (2003) 1960–1961.
- [16] Y. Ma, Y.Q. Huang, Y.W. Cheng, L.J. Wang, X. Li, *Appl. Catal. A-Gen.* 484 (2014) 154–160.
- [17] S. Hu, G.X. Yang, H. Jiang, Y.F. Liu, R.Z. Chen, *Appl. Surf. Sci.* 435 (2018) 649–655.
- [18] M. Chatterjee, H. Kawanami, M. Sato, A. Chatterjee, T. Yokoyama, T. Suzukia, *Adv. Synth. Catal.* 351 (2009) 1912–1924.
- [19] H. Chen, Y.L. He, Lisa D. Pfefferle, W.H. Pu, Y.L. Wu, S.T. Qi, *ChemCatChem* 10 (2018) 2558–2570.
- [20] D.M. Zhang, F.Y. Ye, T. Xue, Y.J. Guan, Y.M. Wang, *Catal. Today* 234 (2014) 133–138.
- [21] J. Matos, A. Corma, *Appl. Catal. A-Gen.* 404 (2011) 103–112.
- [22] C.N. Nicholas, J.S. Manzano, D.S. Aaron, H.O. Steven, I.S. Igor, *ACS Catal.* 5 (2015) 2051–2061.
- [23] Q.Q. Guan, Y.H. Zeng, J.J. Shen, X.S. Chai, J.J. Gu, R.R. Miao, B. Li, P. Ning, *Chem. Eng. J.* 299 (2016) 63–73.
- [24] H.W. Zhang, A.J. Han, K.Z. Okumura, L.X. Zhong, S.Z. Li, S. Jaenicke, G.K. Chuah, *J. Catal.* 364 (2018) 354–365.
- [25] J. He, X.H. Lu, Y. Shen, R. Jing, R.F. Nie, D. Zhou, Q.H. Xia, *Mol. Catal.* 440 (2017) 87–95.
- [26] L. Cheng, Q.G. Dai, H. Li, X.Y. Wang, *Catal. Commun.* 57 (2014) 23–28.
- [27] T.Z. Liu, H. Zhou, B.B. Han, Y.B. Gu, S.Q. Li, J. Zheng, X. Zhong, G.L. Zhuang, J.G. Wang, *ACS Sustain. Chem. Eng.* 5 (2017) 11628–11636.
- [28] C.C. Torres, V.A. Jiménez, C.H. Campos, J.B. Alderete, R. Dinamarca, T.M. Bustamente, B. Pawelec, *Mol. Catal.* 447 (2018) 21–27.
- [29] X. Yang, X. Yu, L.Z. Long, T.J. Wang, L.L. Ma, L.P. Wu, Y. Bai, X.J. Li, S.J. Liao, *Chem. Commun.* 50 (2014) 2794–2796.
- [30] Y.J. Song, H. Wang, X.M. Gao, Y.X. Feng, S.J. Liang, J.H. Bi, S. Lin, X.Z. Fu, L. Wu, *ACS Catal.* 7 (2017) 8664–8674.
- [31] C. Huang, X. Yang, H. Yang, P.Y. Huang, H.Y. Song, S.J. Liao, *Appl. Surf. Sci.* 315 (2014) 138–143.
- [32] S. Velua, M.P. Kapoor, S. Inagaki, K. Suzuki, *Appl. Catal. A-Gen.* 245 (2003) 317–331.
- [33] Y.Q. Wang, J.C. Zhou, X.F. Yang, *Chin. J. Process Eng.* 6 (2009) 1186–1191.
- [34] J.C. Zhou, X.F. Yang, Y.Q. Wang, W.J. Chen, *Catal. Commun.* 46 (2014) 228–233.
- [35] J.Q. Si, W.B. Ouyang, Y.J. Zhang, W.T. Xu, J.C. Zhou, *Sci. Rep.-UK* 7 (2017) 1254.
- [36] Y.J. Zhang, J.C. Zhou, J.Q. Si, *RSC Adv.* 7 (2017) 54779–54788.
- [37] L.H. Chagas, C.R.V. Matheus, P.C. Zonetti, L.G. Appel, *Mol. Catal.* 458 (2018) 272–279.
- [38] S.W. Liu, S. Tan, W.X. Li, J. Song, H.L. Yu, Y. Liu, Q. Wu, S.T. Yu, F.S. Liu, Z.Q. Song, *Mol. Catal.* 458 (2018) 106–111.
- [39] S.S. Ding, C.H. Zhang, Y.F. Liu, H. Jiang, W.H. Xing, R.Z. Chen, *J. Ind. Eng. Chem.* 46 (2017) 258–265.
- [40] Y.T. Hao, L. Li, D. Liu, H.L. Yu, Q. Zhou, *Mol. Catal.* 447 (2018) 37–46.
- [41] Y. Wang, J. Yao, H.R. Li, D.S. Su, M. Antonietti, *J. Am. Chem. Soc.* 133 (2011) 2362–2365.
- [42] Q.Q. Guan, B. Wang, X.S. Chai, J. Liu, J.J. Gu, P. Ning, *Fuel* 205 (2017) 130–141.
- [43] X.T. Liu, F. Pang, J.P. Ge, *Chem.-Asian J.* 13 (2018) 822–829.
- [44] M.S. Zhao, J.J. Shi, Z.Y. Hou, *Chin. J. Catal.* 37 (2016) 234–239.